Journal of the Electrochemical Society

The Use of Chromium and Chromium (III) Oxide PVD Coatings to Resist the Corrosion Driven Coating Delamination of Organically Coated Packaging Steel

Journal of The Electrochemical Society, 2020 **167** 141506

The Use of Chromium and Chromium (III) Oxide PVD Coatings to Resist the Corrosion Driven Coating Delamination of Organically Coated Packaging Steel

N. Wint,[1,z] D. J. Warren,[1] A. C. A. DeVooys,[2] and H. N. McMurray[1]

[1]*Materials Research Centre, College of Engineering, Swansea University, Swansea SA1 8EN, United Kingdom*
[2]*Tata Steel Research and Development, 1970 CA Ijmuiden, The Netherlands*

This paper describes a systematic study into the role of chromium and chromium (III) oxide thickness in preventing corrosion driven coating disbondment of organically coated packaging steel. A graded wedge of chromium and chromium (III) oxide is applied to steel using physical vapour deposition (PVD). A polyvinyl butyral (PVB) overcoat is applied and corrosion is initiated from an artificial defect using NaCl. Scanning Kelvin probe (SKP) potentiometry is used to monitor coating delamination. Wedge thickness variation allows for high throughput investigations into the effect of both metallic chromium and chromium (III) oxide thickness, on coating disbondment rate. A linear reciprocal relationship is observed between chromium metal thickness and disbondment rate. Increasing chromium (III) oxide thickness (applied over chromium metal) results in a decrease in delamination rate. This work highlights the ability of PVD to produce chromium/chromium (III) oxide corrosion resistant coatings to use as alternatives to hexavalent chromium-based systems.
 [DOI: 10.1149/1945-7111/abc360]

Manuscript submitted August 24, 2020; revised manuscript received October 15, 2020. Published November 5, 2020. *This was Paper 2287 presented at the Honolulu, Hawaii, Meeting of the Society, October 7–12, 2012. This paper is part of the JES Focus Issue on Characterization of Corrosion Processes in Honor of Philippe Marcus.*

Packaging materials such as electro chromium coated steel (ECCS) or tin free steel (TFS) are commonly used in food applications to produce can ends and 2 piece cans. They consist of a low carbon, low gauge (0.13–0.49 mm) steel substrate covered in a chromium metal and hydrated chromium oxide layers and are traditionally produced using hexavalent chromium based chromic acid electrolyte baths.

The replacement of the hexavalent chromium used in such baths is an area of much current research due to health and environmental concerns.[1–5] Trivalent chromium-based coatings are one proposed alternative, both for packaging and decorative applications.[5–9] Investigation into the use of trivalent chromium conversion coatings (TCC) for aluminium alloys began in the 1990 s[10–15] and trivalent chromium chemistries have been commercialized for use with aluminium alloys,[16] and by coating suppliers such as Henkel (Alodine T 5900 RTU) and Socomore (Socosurf TCS).[17,18]

Chromium based coatings are typically applied to provide corrosion resistance to packaging steel substrates, which have been shown to corrode in the case that that they are exposed during the can making deformation process.[19] An organic topcoat is therefore commonly added to enhance protection. In the case that the organic overcoat is damaged, creating a defect, the metal substrate can become exposed and atmospheric corrosion of the external surface of the packaging may occur. Organic coating delamination is subsequently of significant interest when considering novel packaging materials.

During the corrosion driven cathodic delamination, the rate at which the organic coating becomes detached from the metal substrate is limited by the cathodic reaction, commonly the cathodic oxygen reduction reaction (ORR), given by Eq. 1. Anodic metal dissolution at an organic coating defect is coupled to the ORR, which occurs at the delamination front, by a thin $<5\,\mu$m electrolyte.[20] The susceptibility of ECCS replacements to the ORR is therefore of importance.

$$O_2 + 2H_2O + 4e^- \rightarrow 4OH^- \qquad [1]$$

The electrolyte bath chemistry has been found to have a significant effect on final coating composition.[5–9,21–23] For example, the conductivity of chromium (III)-based coatings, applied using electroplating, has been found to fall in the case that chromium hydr (oxide) forms.[22] Furthermore, a decreased rate of ORR has been reported in the presence of both Cr $(OH)_3$[23] and Cr_2O_3,[24] this being attributed to the reduced rate of electron transfer through thin oxide films,[25] which has been found to decrease exponentially with increasing coating layer thickness.[26] The corrosion driven cathodic disbondment of a PVB coating from production line chromium (III) metal-oxide-carbide coated steel has been shown to decrease with increased chromium (III) oxide content in previous work.[27] However, in that work, the total chromium (III) metal-oxide-carbide coating thickness was also varied, and the effect of chromium (III) oxide thickness was not investigated in isolation.[27] The role that chromium hydr(oxide), present within chromium-based coatings, plays in determining the rate of the ORR, and thus corrosion driven coating disbondment, is therefore of interest when considering design of alternatives to traditional coatings.

Small variations in the chemistry of the electroplating bath can result in changes in the properties of electroplated packaging materials and reduced corrosion performance. Alternatives to electroplating, such as physical vapour deposition (PVD) can offer greater control over coating properties and should be considered as an application process which can be used in cases that coating composition is critical. PVD has been considered as a "clean" alternative by which to apply protective and decorative coatings and offers savings with respect to both energy and waste.[28–30] Previous work has compared the performance of thin chromium films that have been applied via PVD and electroplating.[31] PVD is subsequently considered a suitable method by which to apply chromium metal and chromium (III) oxide coatings of controlled thicknesses, with the aim of systematically studying the independent role that each coating component plays in the prevention of cathodic delamination. The ability to sputter multilayer Cr/C_2O_3 films[32] and corrosion resistant Cr_2O_3 plasma coatings[33] has been demonstrated elsewhere.

The intention of the current work is therefore to build upon the findings obtained that showed that corrosion driven cathodic disbondment of a PVB coating, from production line chromium (III) metal-oxide-carbide coated steel, decreased with increased chromium oxide thickness. It does so by following a methodology used previously for aluminium[34] and magnesium based coatings,[35] to apply a chromium and chromium (III) oxide wedge of graded thickness to a steel substrate using PVD. This allows one to

[z]E-mail: n.wint@swansea.ac.uk

determine the specific role that either the metallic chromium layer thickness (t_{Cr}), or 2.) chromium (III) oxide thickness (t_{ox}) plays in determining the rate of corrosion-driven coating disbondment. In so doing, the disbondment of an electrically non-conducting polyvinybutyral (PVB) overcoat will be investigated using scanning Kelvin probe (SKP) potentiometry. The ability of the SKP apparatus to study the corrosion driven cathodic delamination of coatings has been shown elsewhere.[36–40] The results will allow determination of the optimum coating composition and thickness with the aim of identifying the lowest coating thickness necessary to provide resistance to coating delamination at minimal cost.

Experimental

Materials.—Sheets of low alloy T61 grade mild steel of 0.2 mm gauge, along with electrolytic chromium coated steel (ECCS) were obtained from Tata Steel UK. The ECCS sample consisted of the T61 grade steel with the addition of a ~30 nm chromium/hydrated chromium oxide coating. The chromium deposition sources used for PVD were acquired from Kurt J Lesker and were of at least 99.2% purity. Polyvinyl butyral-co-vinyl alcohol-co-vinylacetate (PVB), molecular weight 70,000–100,000 Da and all other chemicals were obtained from Sigma Aldrich Chemical Co. at analytical grade purity.

Methods.—Samples were cut from larger steel sheets and were polished using Buehler 5 μm abrasive alumina powder before being rinsed using distilled water and ethanol.

Thin metallic layers were sputtered on to the steel substrate using a Kurt J Lesker PVD75 Physical Vapour Deposition system following a procedure described previously to apply aluminium[34] and magnesium[35] PVD wedge coatings. Samples were attached to the sample holder using countersink head machine screws in order to keep them flat. Vacuum compatible polyimide tape (CHR K250 Saint-Gobain Performance Plastics) was used to expose an area on which to deposit the film. The sample holder was then placed in the vacuum chamber of the PVD system such that it could not obstruct the sliding shutter mechanism, that was used to apply films of variable thickness. A pressure was maintained at 3×10^{-3} Torr during deposition (the base pressure of the vacuum pump was 5×10^{-8} Torr). Prior to deposition the surface of the samples underwent a plasma etch for 20 min. An argon gas flow rate of 100 standard cubic centimetres (SCCM) per minutes and an applied power of 60 Watts were employed.

To avoid depositing surface oxide from the target the first 5 min of a deposition was carried out onto the shutter until the deposition rate stabilized. In the case of duplex chromium/chromium (III) oxide coatings, a 500 nm thick planar chromium metal layer was firstly applied to the steel substrate. The addition of oxygen to the PVD chamber has previously been found to result in the production of metal oxide coatings. As such, 3 SCCM of O_2 equivalent in the ratio 1:10 oxygen to argon during the sputtering of chromium[41,42] to produce the overlying Cr (III) layer.

For application of both the Cr and Cr(III) oxide wedge coatings, the shutter was positioned in such a way that it covered the entirety of the exposed area (Fig. 1) at the start of the deposition process. The rate at which the shutter was withdrawn, and thus the rate at which the film thickness varied was controlled using Eq. 2, where v is the shutter speed, w is the width of the area to be coated, T is the maximum film thickness required, and D is the deposition rate.

$$v = \frac{w}{T/D} \qquad [2]$$

The shutter moved until all of the unmasked area was exposed and deposition was stopped. The argon gas flow rate used was 30 SSCM and the power was 250 W. The mass deposition rate was determined using a sigma instruments oscillating crystal microbalance. The microbalance was used to estimate a mass (per unit area) deposition rate. The coating weight is then given by the product of mass deposition rate and deposition time. The sliding shutter varies deposition time in a linear fashion, that allows the coating weight to be estimated at every point in the resulting film deposit "wedge." Using density values tabulated for the relevant material, the thickness of the PVD film may then be calculated from the coating weight at any point. In the case of chromium metal coatings, the density was assumed to be that of bulk metal. The theoretical density value used for chromium oxide coatings assumes the deposition of a stochiometric, perfectly crystalline layer. In reality, the chromium oxide PVD deposit is likely to be significantly defective and the calculated coating thickness is therefore likely to represent a minimum estimate. A rate of 2–3 Å.s^{-1} was achieved throughout.

Corrosion driven coating disbondment was investigated using a "Stratmann" type cell, as shown in Fig. 2.[36–40] Following application of the PVD coatings, a 15 mm × 50 mm strip of clear adhesive tape was applied across one end of the sample, parallel to the coating wedge profile. Two parallel strips of insulating tape were attached to the coupon, perpendicular to the clear adhesive tape. An ethanolic solution (15.5 wt.%) of PVB was bar cast on the area that remained, the insulating tape acting as a height guide. In all cases the PVB used was unpigmented. Although PVB does not fully represent industrial coating systems, it was used in the current work as it allows a measurable degree of delamination over a short time-scale. It is therefore considered to be a suitable alternative when the principal aim is the comparison of substrates with respect to their ability to resist corrosion driven coating disbondment of organic coatings. The dry film thickness was 30 μm as measured using a micrometer screw gauge. The clear tape was then partially peeled back to expose a 15 mm × 20 mm area of bare metal, that acted as an artificial PVB coating defect. A barrier between the intact coating and defect area was formed by the residual clear adhesive tape and PVB overcoating. The remaining sides of the defect were lined with non-corrosive silicone rubber and a 2 cm^3 volume of 0.86 mol.dm^{-3} aqueous NaCl electrolyte was applied to initiate corrosion.

Calibration of the SKP, needed to convert Volta potential values recorded to corrosion potential (E_{corr}) has been described in detail previously.[36–40] The Volta potential difference above metal (Ag, Cu, Fe and Zn) wells filled with 0.5 mol.dm^{-3} aqueous solution of the respective metal chloride salt (nitrate salt in the case of Ag) was measured by the SKP. The values obtained were compared to the metal electrode potential values that were simultaneously measured vs SCE using a Solartron 1280 potentiostat.

Reservoirs of 0.86 mol.dm^{-3} aqueous NaCl were used within the SKP chamber to ensure a constant humidity of ca. 93% RH and the temperature was maintained at 25 °C. The SKP gold wire (125 μm diameter) probe was scanned along a 12 mm line, perpendicular and contiguous to the defect/coating interface. The probe was positioned at a constant height of 100 μm above the sample. The sample was scanned immediately after application of the aliquot of electrolyte to the defect and subsequent scans took place at intervals of 1 h. E_{corr} values were taken at regular intervals along individual lines (dotted lines in Fig. 2) in such a way that that each line represented a different coating thickness value. The number of scan lines was based on the lateral resolution L of the SKP (Eq. 3), where d is probe-specimen distance and D is the probe diameter.[43] For this work, d = 100 μm and D = 125 μm. The lateral resolution, according to Eq. 3, will be ~140 μm. The number of lines was therefore chosen to maximise the amount of chromium thickness values, whilst ensuring that the inter line spacing was greater than 140 μm, and therefore that the Volta potential values recorded for each scan line were not influenced by the adjacent scan line (for which Cr thickness would be substantially different).

$$L = 0.884d + 0.4D \qquad [3]$$

Results

Cathodic delamination of chromium coatings.—To establish baseline delamination kinetics, the cathodic disbondment of PVB

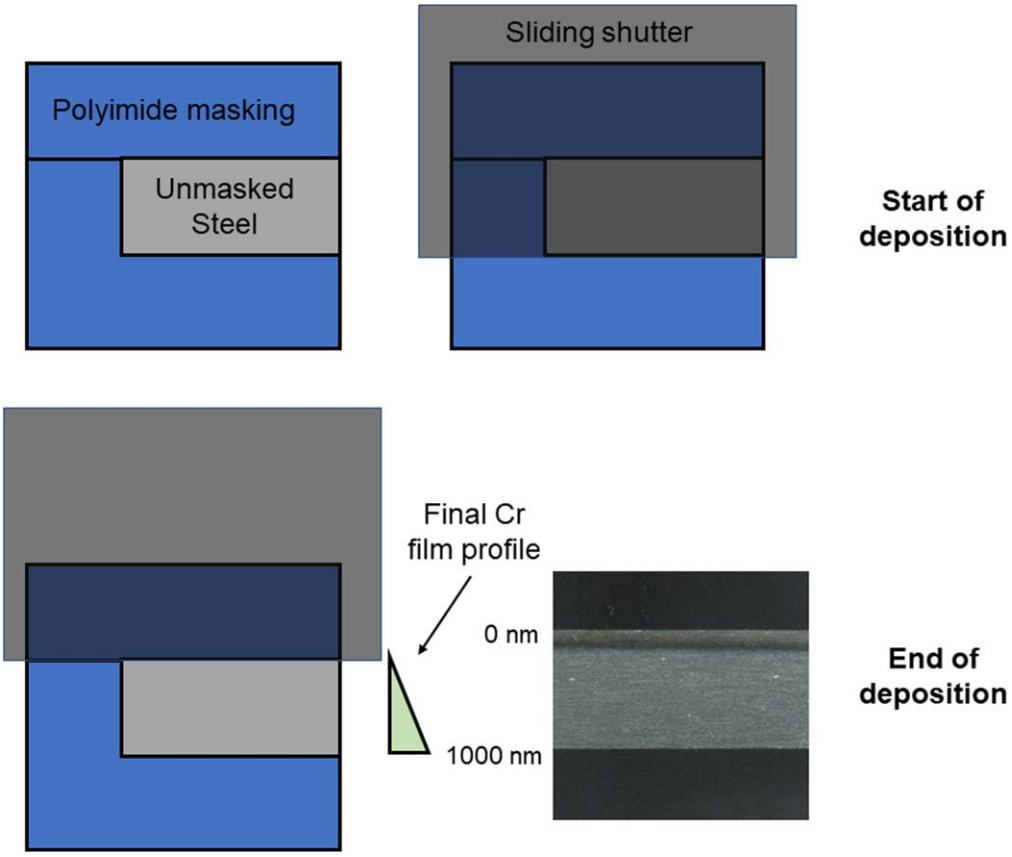

Figure 1. Schematic representation of (a.) the process by which a graded wedge coating is formed using a sliding shutter mechanism and (b.) the finished wedge coating produced in the case of a chromium coating.

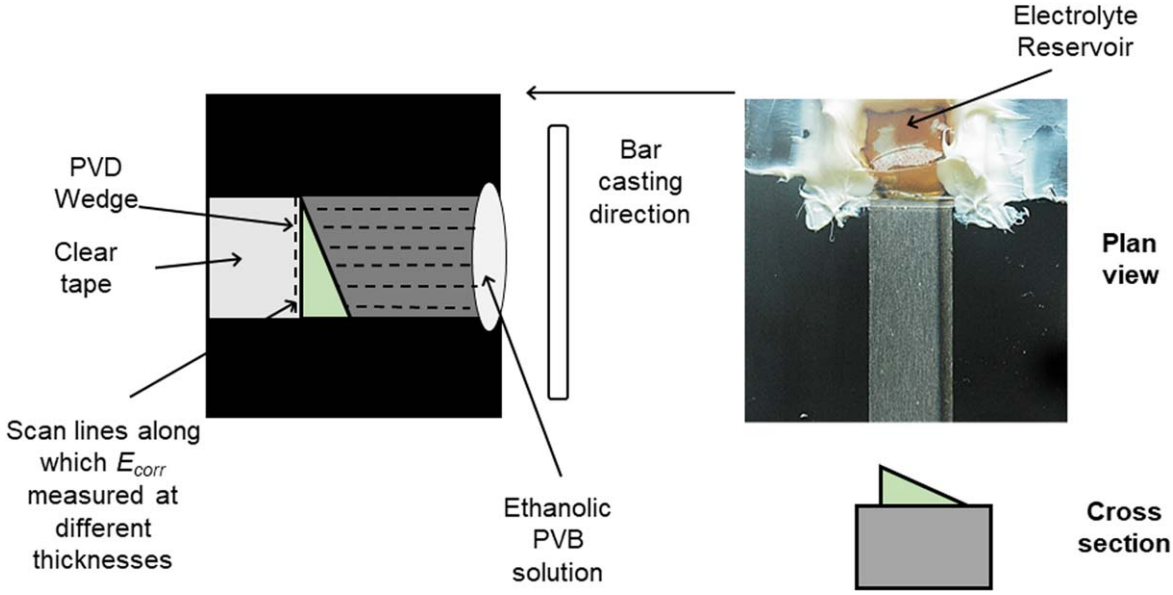

Figure 2. Schematic representation of (a.) the use of masking tape and PVB to produce a "Stratmann" cell and (b.) the sample configuration for study of corrosion driven coating disbondment using in situ SKP.[34]

from a plain steel substrate was monitored using the SKP. Time-dependent $E_{corr}(x)$ profiles (shown in Fig. 3) became established within ca. 120 min of the electrolyte being introduced into the defect region and are typical of those described previously.[36–40] The potential value associated with the undelaminated, intact coating remains constant at a value of ca. 0.1 V vs SHE.[36–40] The potential values measured are ~ -0.4 V vs SHE within the defect region are consistent with those expected for freely corroding iron (-0.44 V vs SHE), both these values being consistent with measurements made previously.[36–40] The anodic activity at the artificial coating defect is coupled to the cathodic oxygen reduction reaction (ORR) at the delamination front. The products of the ORR, OH^- or reactive

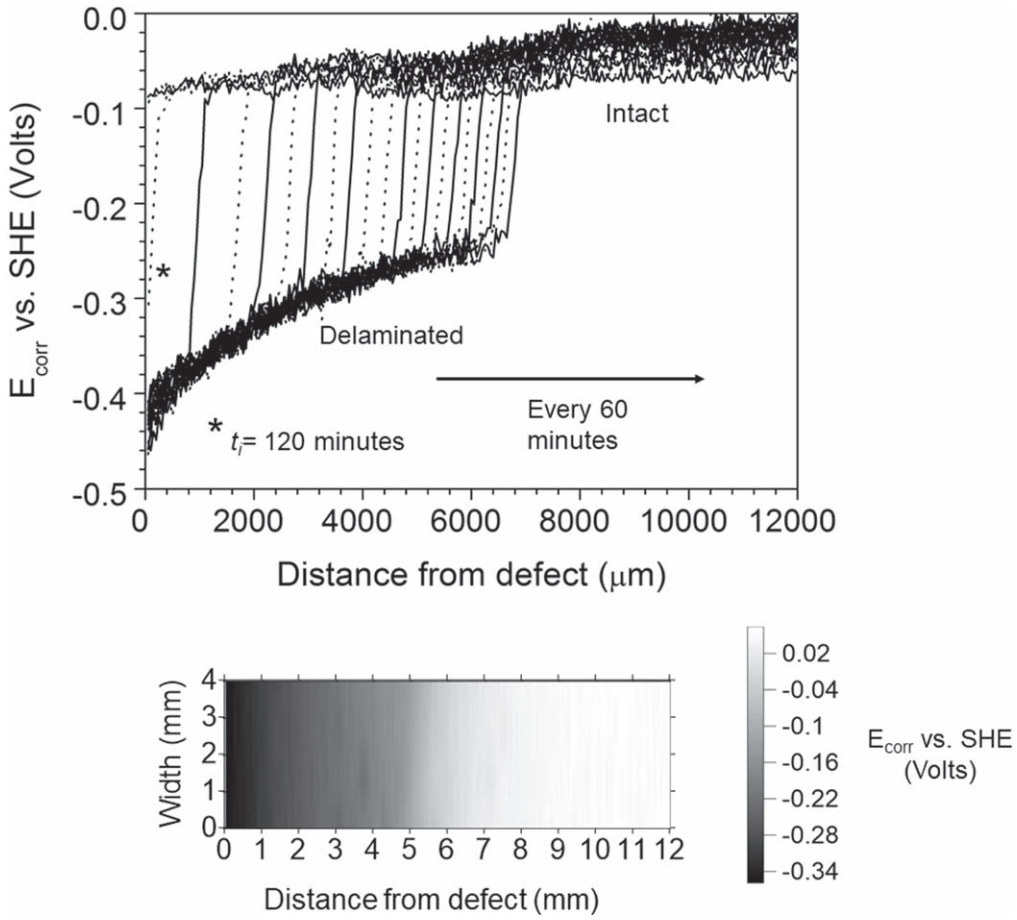

Figure 3. SKP derived E_{corr} as a function of distance from defect *(x)* profiles for the delamination of a PVB model coating from a steel substrate after initiation using a 0.86 M NaCl electrolyte. Key: (*) 120 min after initiation with 0.86 mol.dm^{-3} NaCl and 60 min intervals thereafter. Also shown is a Fig. 3 also shows a false colour map of the E_{corr} values obtained 12 h after the electrolyte is introduced into the defect.

intermediates, are believed to attack the bond between the PVB coatings and metallic substrate, this resulting in loss of coating adhesion.[37] The sharp increase in potential that occurs at the boundary between the delaminated and intact coating can be used as a semi-empirical means by which to locate the position of the delamination front.[36–40] Figure 3 also shows a false colour map of the E_{corr} obtained 12 h after the electrolyte was introduced into the defect. The defect is positioned at the left hand side of the map and the coating therefore delaminates from left to right, as indicated. The potential within the regions where the coating has delaminated (represented by the darker regions) is similar to that shown in the time dependent profiles. The areas in which the coatings are intact (lighter) are associated with higher potentials of ca. 0.1 V vs SHE. The coating appears to have delaminated a distance of ~5 mm at this time point. The delamination front is uniform across the 4 mm width of the scanned area.

A chromium wedge was applied to a steel substrate, with the aim of determining the role of chromium in preventing the cathodic disbondment of organic overcoats. The value of t_{cr} varied from 0 nm to 1000 nm across the wedge. The variation in delamination rate with t_{cr} can be seen clearly in Fig. 4 that shows three false colour maps of the E_{corr} at various times after initiation of coating delamination. The defect is positioned at the left hand side of each map and the coating therefore delaminates from left to right, as indicated. As with Fig. 3, the sharp increase in potential that occurs at the boundary between the delaminated coating and intact coating can be used as a semi-empirical means by which to locate the position of the delamination front.[36–40] The potential within the regions where the coating has delaminated (represented by the darker regions) is ca. −0.3 V vs SHE. The areas in which the coatings are intact (lighter) are associated with higher potentials of ca. 0.2 V vs SHE. In the case of the thickest coatings (bottom of each colour map) the distance over which the coating has delaminated after 12 h is approximately 4.5 mm. In comparison, the distance of the delamination front from the defect in the case of the thinnest coatings is ca. 8 mm distance. After 17 h the thinnest part of the coating has delaminated across the entire scanned region, whilst the thickest part of the coating has delaminated ~5.5 mm, reaching ~8 mm after 22 h. The position of the delamination front changes across the width of the sample, and thus with coating thickness. This is in direct contrast to the uniform front observed in Fig. 3.

Figures 5a and 5b show time-dependent $E_{corr}(x)$ profiles obtained by extracting the E_{corr} values measured along each scan line (where each scan line is associated with a different t_{cr}value) when t_{cr} is 100 nm (Fig. 5a) and 1000 nm (Fig. 5b). Comparison of Fig. 3 with Fig. 5 indicates that the presence of chromium does not significantly change the E_{corr} profiles from those observed in the case of a plain steel substrate. Whilst the time before initiation appears to increase from (120 ± 60) min in the case of plain steel, to (288 ± 60) min in the case of t_{cr} = 1000 nm chromium coatings, it should be remembered that the SKP is incapable of measuring Volta potential values immediately up to the defect. The initiation time (time at which first E_{corr} profile detected) is therefore associated with some error. The E_{corr} values associated with t_{cr} = 100 nm are similar to those obtained in the case of t_{cr} = 1000 nm. Parabolic kinetics, consistent with cation migration control are observed in both cases. By the end of the 24-hour experimental time period the 100 nm coating fully delaminated from the 12 mm region of interest. In

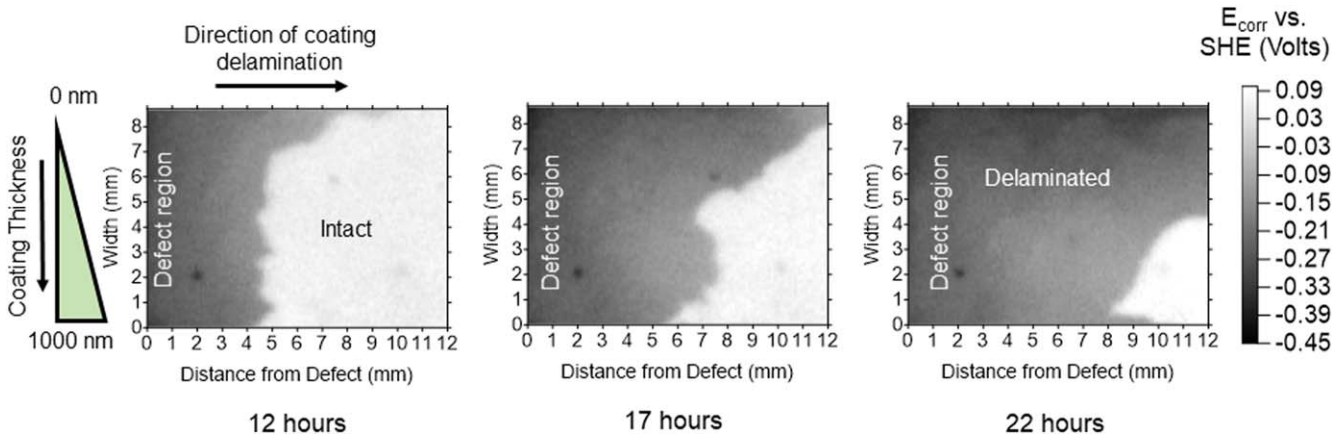

Figure 4. A false colour map of SKP derived E_{corr} values obtained during the delamination of a model PVB coating from a PVD chromium wedge coated steel substrate. t_{CR} varies from 0 nm (top) to 1000 nm (bottom). Measurements were taken 12 h, 17 and 22 h after initiation using a 0.86 mol.dm^{-3} NaCl electrolyte.

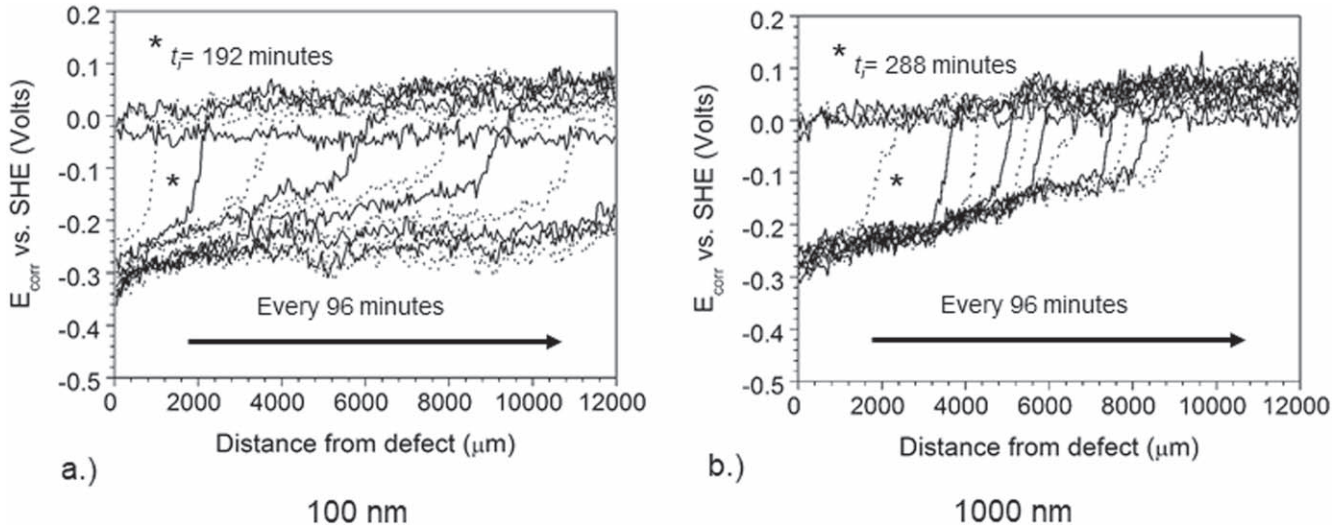

Figure 5. SKP derived E_{corr} as a function of distance from defect *(x)* profiles for the delamination of a PVB model coating from PVD chromium wedge coated steel substrate after initiation using a 0.86 mol.dm^{-3} NaCl electrolyte where $t_{CR}$is (a.) 100 nm and (b.) 1000 nm. Key: (a.) (*) 192 min and (b.) 288 after initiation. Profiles are shown at intervals of 96 min thereafter.

comparison the delamination front has only reached a distance of ca. 9 mm from the coating defect region in the case of 1000 nm thick coatings.

The time-dependent distance of the delamination front from the artificial defect (x_{del}) can be acquired by detecting the point at which the highest potential gradient in the relevant E_{corr} profiles (shown in Fig. 5) occurs.[36–40] Values of x_{del} can then be plotted as a function of the delamination time t_{del} with which it is associated (Fig. 6) and the delamination kinetics can be investigated. For unpigmented PVB coatings, migration of cations (here Na^+) within the underfilm electrolyte has been found to control the rate of coating disbondment.[37–39] Delamination kinetics are parabolic follow Eq. 4, where k_d is the parabolic delamination rate constant and t_i is the delamination initiation time.

$$x_{del} = k_d(t_{del} - t_i)^{\frac{1}{2}} \quad [4]$$

The initial rate of coating delamination was used for purposes of comparison. Initial rates were estimated using a least squares regression method. The values obtained are shown in Table I. Values shown are based on the average of at least three readings and error intervals represent one standard deviation on the mean.

The k_d values obtained using Fig. 6 were plotted as a function of t_{cr} and are shown in Fig. 7. An almost linear reciprocal relationship exists between k_d and t. Despite the improvement in cathodic

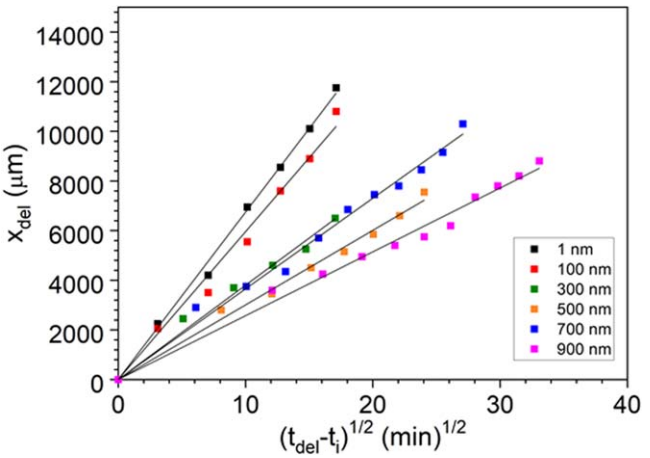

Figure 6. Plots of delamination distance x_{del} vs $(t_{del}\text{-}t_i)^{1/2}$ for the disbondment of a model PVB coating from a PVD chromium wedge coated steel substrate.

delamination resistance offered by chromium coatings at higher t_{cr} values, mass transport remains rate determining and coating failure is not limited by a significant amount.

Table I. SKP derived delamination rate constant k_d obtained for the delamination of a PVB coating from steel coated with varying thickness of a chromium PVD layer.

PVD Cr layer thickness (nm) t_{CR}	$k_d(\mu m.min^{-1/2})$
1000	171 ± 6
900	255 ± 10
800	302 ± 16
700	357 ± 12
600	359 ± 12
400	414 ± 50
200	570 ± 64
100	614 ± 28
1	681 ± 18

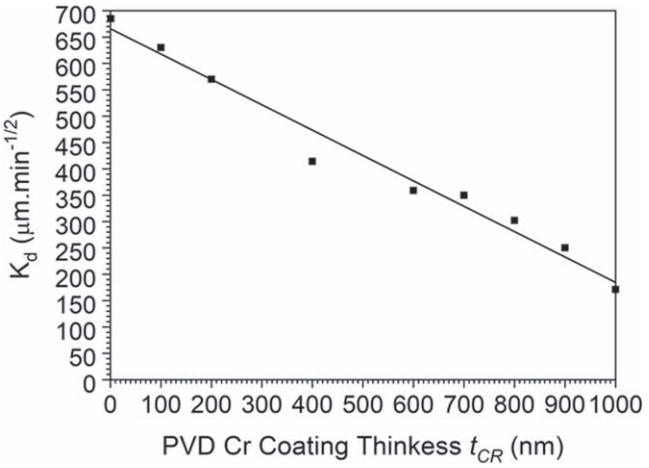

Figure 7. The parabolic delamination rate constant k_d as a function of chromium thickness t_{CR} for the delamination of a PVB model coating from PVD chromium wedge coated steel substrate after initiation using a 0.86 mol.dm^{-3} NaCl electrolyte. k_d obtained from Fig. 6.

Cathodic delamination of chromium oxide coatings.—As previously mentioned, ECCS is commonly used throughout the packaging industry, and consists of a steel substrate covered in a chromium and hydrated chromium oxide layer. A PVB coating did not delaminate from an ECCS substrate over the 96 h time period for three repeat experiments. The absence of coating disbondment is made evident in Fig. 8 that shows profiles of E_{corr} vs distance from the penetrative defect, obtained at various times. It may be seen from Fig. 8 that potential values recorded using the SKP show a time-dependent evolution but tend to stabilize as time increases. Thus, initially, values of E_{corr} measured over the intact (un-corroded) surface (E_{intact}) increase progressively with time but tend toward an approximately constant value of 0.06 ± 0.02 V vs SHE. The physicochemical processes influencing E_{intact} have been described at length elsewhere.[44] Briefly, introduction of the sample into the SKP chamber is expected to result in: 1.) hydration of the PVB coating, which comes into isopiestic equilibrium with the humid chamber atmosphere and 2.) the onset of through-coating oxygen reduction and interfacial metal oxidation reactions, which establish a mixed potential. These electrochemical reactions do not come into equilibrium but will tend towards a steady-state as time increases. It therefore seems reasonable to assume that the time-dependent evolution in E_{intact} observed in Fig. 8 results from a transient oxidation of the reactive iron surface at the iron-PVB interface occurring after the coated sample has been introduced to the humid SKP chamber environment.[44]

The corrosion protection offered by Cr based coatings is attributed to the formation of passive chromium oxide, the nature

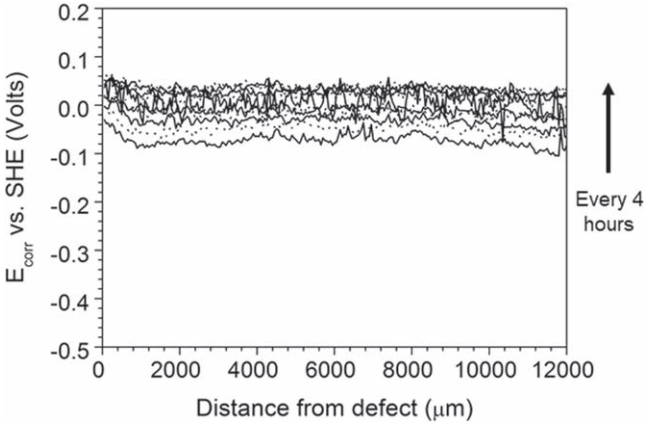

Figure 8. SKP derived E_{corr} as a function of distance from defect *(x)* profiles recorded over a 48 h period for the delamination of a PVB model coating from a ECCS after initiation using a 0.86 mol.dm^{-3} NaCl electrolyte.

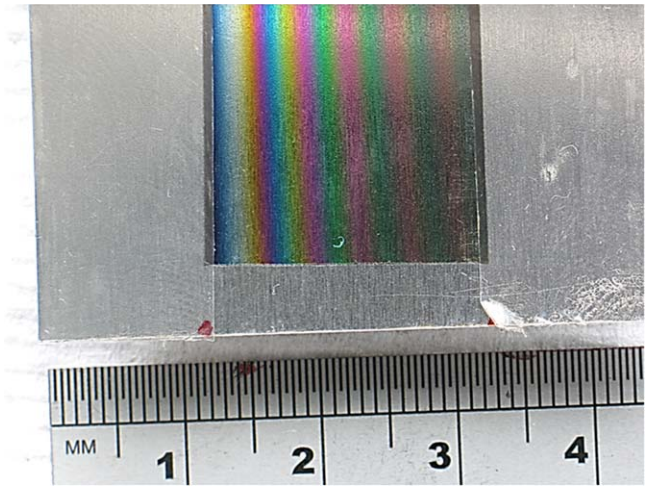

Figure 9. An optical image of a steel sample covered in 500 nm of chromium metal and a 200 nm chromium oxide wedge.

of which differs to that of the chemically grown hydrated chromium oxide present in the case of ECCS. The resistance to cathodic delamination offered by a chromium oxide layer, when compared to that offered by ECCS is therefore of interest and the effect of t_{OX} on the rate of PVB disbondment was therefore investigated. The value of t_{cr} was kept constant at 500 nm. A chromium (III) oxide wedge overlayer was then applied. Figure 9 shows an optical image of the sample surface following application of a chromium (III) oxide wedge. Colourful thin-film interference patterns are clearly visible, this providing evidence that the oxide thickness is comparable to the wavelength of visible light.[45]

The variation in coating delamination rate with t_{OX} can be seen clearly in Fig. 10 which shows three false colour maps of the E_{corr} measured at various times after initiation of coating delamination. The defect is positioned at the left hand side of each map and the coating therefore delaminates from left to right, as indicated. As with Fig. 4, the potential within the regions where the coating has delaminated (represented by the darker regions) is ca. −0.3 V vs SHE. The areas in which the coatings are intact (lighter) are associated with higher potentials of ca. 0.2 V vs SHE. In the case of the thickest coatings (200 nm) at the top of each image (note this is in contrast to Fig. 4 when the thickest coatings are at the bottom of the image), the coating remains intact over the entire length of the scan line at each of the three time points. In comparison the distance of the delamination front from the defect in the case of the thinnest coatings is ca. 4 mm after 48 h.

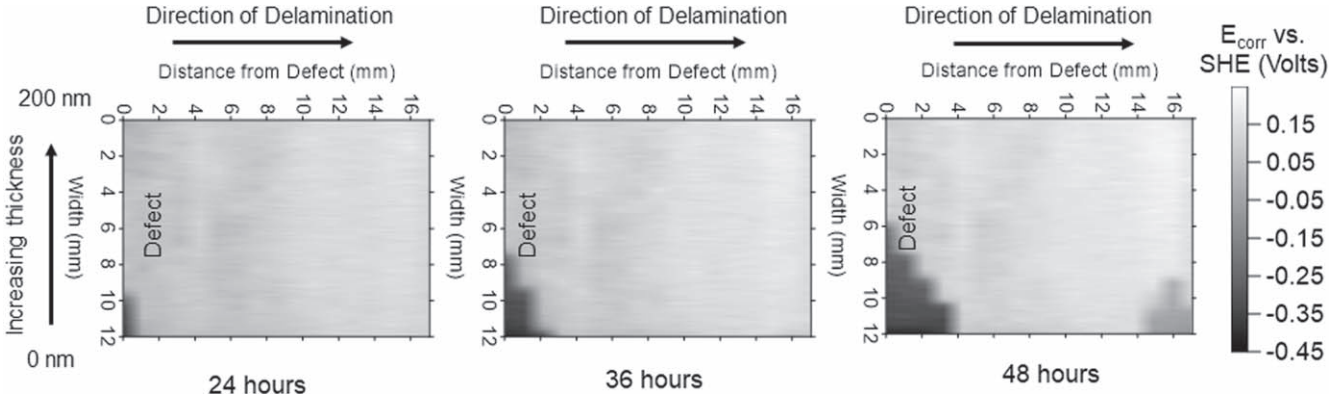

Figure 10. A false colour map of SKP derived E_{corr} values obtained during the delamination of a model PVB coating from a PVD chromium (III) oxide wedge/chromium coated steel substrate. $t_{CR} = 500$ nm and t_{OX} varies from 0 nm (right) to 200 nm (left). Measurements were taken after 24, 36 and 48 h after initiation using a 0.86 mol.dm^{-3} NaCl electrolyte.

As with Fig. 3, the sharp increase in potential that occurs at the boundary between the delaminated coating and intact coating can be used as a semi-empirical means by which to locate the position of the delamination front.[36–40] The potential within the regions where the coating has delaminated (represented by the darker regions) is ca. −0.3 V vs SHE. The areas in which the coatings are intact (lighter) are associated with higher potentials of ca. 0.2 V vs SHE. In the case of the thickest coatings (bottom of each colour map) the distance over which the coating has delaminated after 12 h is approximately 4.5 mm. In comparison, the distance of the delamination front from the defect in the case of the thinnest coatings is ca. 8 mm distance. After 17 h the thinnest part of the coating has delaminated across the entire scanned region, whilst the thickest part of the coating has delaminated ∼5.5 mm, reaching ∼8 mm after 22 h.

Figure 11 shows a plot of delamination distance (x_{del}) vs t for the disbondment of a model PVB coating from Cr (III) oxide PVD wedge/chromium coating where t_{CR} is 500 nm and t_{OX}varies from 10 to 200 nm. A parabolic relationship, consistent with mass transport limited behaviour is observed in the case that $t_{OX} <$ 120 nm. When $t_{OX} = 180$ nm, a linear relationship is observed, this being indicative of electron transfer control and suggests that the Cr (III) oxide layer is able to reduce the rate at which electrons travel to the cathode, thus stifling the ORR. The k_d values obtained from Fig. 11 are shown in Table II, and show that the t_{cr} does not have a significant effect on the delamination rate. Values shown are based on the average of at least three readings and error intervals represent one standard deviation on the mean. Figure 11 also shows that the initiation time increases significantly from 100 min when $t_{OX} = 0$ nm to 2100 min when $t_{OX} = 180$ nm. At this point it should again be borne in mind that the SKP is unable to measure Volta potential values immediately up to the defect. Any difference in delaminated distance observed in Fig. 10 is therefore believed to be a consequence of the increase in initiation time with increasing t_{OX}, as opposed to a variation in delamination rate.

A question arises as to why, in the combinatorial experiment, the organic coating cathodic delamination rate appears to be largely independent of Cr (III) oxide thickness on an iron substrate (Table II). This finding is in direct contradistinction to that previously reported in the case of MgZn "wedge" combinatorial libraries on a zinc substrate, in which delamination rate decreased dramatically as surface Mg_2Zn_{11} intermetallic layer thickness increased.[35] In the case of both Cr(III) oxide and Mg_2Zn_{11} intermetallic surface layers, the local rate of cathodic O_2 reduction and therefore organic coating delamination rate is expected to decrease as layer thickness increases. One possible explanation is that the invariance of delamination rate on iron results from a lateral (direction normal to the direction of the delamination) diffusion of electrolyte ions (most importantly OH^-) in the thin layer of catholyte that forms beneath the delaminated PVB coating. The iron substrate

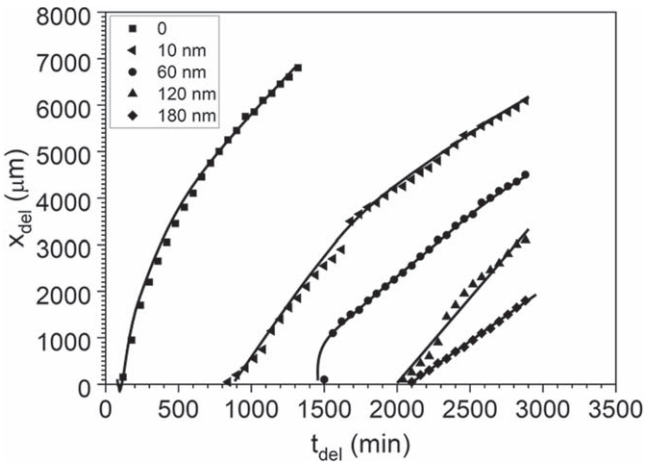

Figure 11. Plots of delamination distance (x_{del}) vs t for the disbondment of a model PVB coating from chromium oxide PVD wedge/chromium coating where t_{CR} is 500 nm and t_{OX} varies from 10–180 nm.

in contact with the underfilm catholyte is predicted to remain passive,[46] and no underfilm anodic activity occurs that might consume the OH^- produced through cathodic O_2 reduction. Consequently, a very high underfilm pH can be produced and values as high as pH 14 have been reported.[20] Proton and hydroxide ion are by far the fastest diffusing ions in liquid water.[47] and the rapid lateral diffusion of OH^- would tend to uniformize underfilm pH across the combinatorial wedge sample. Under these circumstances, increasing Cr(III) oxide thickness might result in a decrease in local cathodic O_2 reduction rates but minimal decrease in local pH. An invariance of delamination rate with Cr (III) oxide thickness would then result if direct chemical attack by OH^- on the PVB coating or coating-metal bond was a major contributor to the coating disbondment mechanism[20,37] The finding that this is not the case for MgZn "wedge" combinatorial libraries on a zinc substrate can then be explained on the basis of the much lower pH (pH 10–11) that evolves beneath the delaminated organic coating on zinc. Zinc is not passive in contact with the underfilm catholyte and underfilm pH becomes moderated through an anodic dissolution of zinc to produce soluble hydrogen zincate or zincate anions.[48,49] Under these circumstances, the lateral diffusion of OH^- and organic coating disbondment through direct chemical attack by OH^- is less likely to be significant and local rates of PVB coating delamination are more completely controlled by local rates of cathodic O_2 reduction.[46]

Glow Discharge Optical Emission Spectroscopy (GDOES) was used to establish the composition of a coating for which $t_{cr} =$ 500 nm and $t_{OX} =$ 200 nm. Figure 12 shows the top 400 nm to

Table II. SKP derived delamination rate constant k_d obtained for the delamination of a PVB coating from steel coated with 500 nm of PVD chromium metal and varying thicknesses of a chromium oxide PVD layer.

PVD Cr layer thickness (nm) t_{cr}	$k_d(\mu m.min^{-1})$
180	2.21 ± 0.02
120	3.81 ± 0.16
60	2.74 ± 0.09
10	3.03 ± 0.08
0 (500 nm PVD Cr)	5.10 ± 0.26

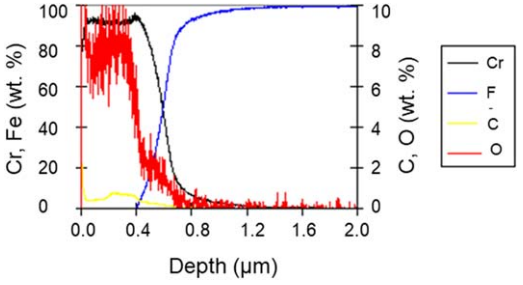

Figure 12. GDOES analysis of a bilayer chromium (III) oxide/chromium metal coating for which $t_{CR} = 500$ nm and $t_{OX} = 200$ nm.

contain ca. 90 wt.% Cr and ca. 8 wt.% O. Although the amount of oxide present is less than that expected in the case of stoichiometric Cr_2O_3 (~30–35 wt.%) the results indicate that chromium oxide is present in the outermost parts of the coating.

To mitigate the effects of crosstalk, a non-combinatorial approach was taken when investigating the role of Cr(III) oxide thickness in preventing cathodic delamination. As such, two different types of planar bi-layer coatings were produced. For both samples $t_{cr} = 500$ nm. In the case of the first sample, this chromium layer was overcoated with a uniform 10 nm chromium (III) oxide layer, and in the case of the second, the chromium (III) oxide layer was 200 nm thick. Figures 13a and 13b show the time-dependent $E_{corr}(x)$ profiles obtained for each sample. The E_{corr} values within the defect and intact region, shown in Fig. 13a, are similar to those obtained in Fig. 5 for chromium coatings.

Figure 13b strongly resembles Fig. 8 and a similar E_{corr} plateau value of 0.1 V vs SHE is recorded. It is therefore clear that the $t_{OX} = 200$ nm is sufficient to prevent cathodic delamination of the PVB coating over at least the 48 h experimental time period and it therefore seems plausible that it is the chromium (III) oxide, the presence of which is confirmed in Fig. 12, which is responsible for the decrease in cathodic delamination rate. The change from mass transport control to electron transfer control when $t_{OX} \leqslant 120$ nm (Fig. 11) is indicative that the chromium (III) oxide is able to offer resistance to coating delamination as a result of its poor electronic conductivity. The resistivity of 140 nm thick Cr_2O_3 films applied using thermal evaporation onto a glass substrate have previously been reported as 4×10^7 Ωcm.[50]

Conclusions

This work has shown that it is possible to produce a chromium and chromium/chromium (III) oxide coating combinatorial library on a single substrate through physical vapour deposition (PVD) of a "wedge" onto a steel substrate. This allows for a rapid, parallel investigation into the role of coating thickness in preventing the corrosion driven coating disbondment of organic coatings from packaging steel, using SKP.

- An almost linear, inverse relationship was observed between chromium coating thickness and parabolic rate constant of cathodic disbondment. The delamination process was controlled by mass transport of cations in the underfilm electrolyte in all cases.
- A 200 nm chromium (III) oxide wedge was applied over a 500 nm thick chromium coating. GDOES was used to confirm the presence of Cr (III) oxide. An increase in chromium (III) oxide coating thickness resulted in a dramatic decrease in cathodic delamination rate. At thickness values ⩾120 nm kinetics became controlled by electron transfer.
- The delamination rate constants obtained for each Cr (III) oxide thickness were similar. This was believed to be a result of the lateral diffusion of electrolyte ions that can occur once the PVB coating has started to delaminate. Lateral OH^- diffusion would result in increased coating delamination rates. A non-combinatorial approach, whereby bi-layer (500 nm chromium metal overlayed with chromium oxide) planar samples were produced, was subsequently adopted.
- For the case that chromium (III) oxide thickness was 200 nm, cathodic delamination was not observed for the 48 h experimental time period. This also was also the case for traditional electroplated

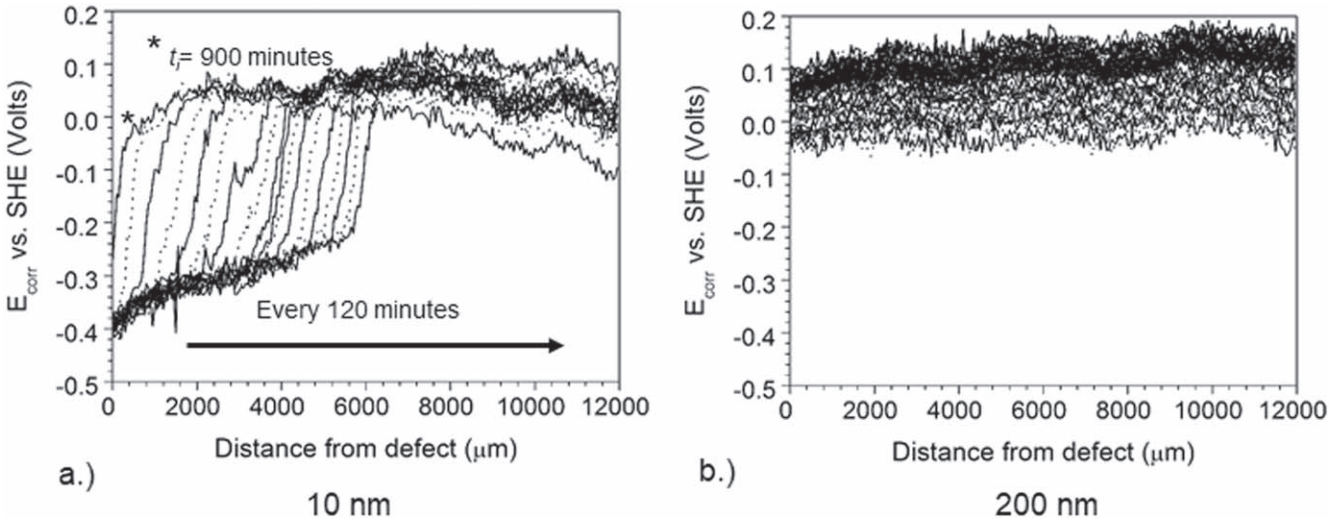

Figure 13. SKP derived E_{corr} as a function of distance from defect (x) profiles recorded for 48 h for the delamination of a PVB model coating from PVD chromium (III) oxide wedge/chromium coated steel substrate after initiation using a 0.86 mol.dm^{-3} NaCl electrolyte where t_{CR} is 500 nm and t_{OX} (a.) 10 nm and (b.) 200 nm. Key: (a.) (*) 900 min after initiation with 0.86 M NaCl and 120 min intervals thereafter and (b.) for a total experimental time period of 48 h.

chromium/hydrated chromium oxide coatings produced using hexavalent chromium.

- The ability of chromium (III) oxide to resist coating failure at a thickness of 200 nm is believed to be a result of the low electronic conductivity, and therefore the low rate of electron transfer, associated with Cr_2O_3.
- This work highlights the benefits of using chromium (III) oxide when developing delamination resistant alternatives to hexavalent chromium based coating systems for packaging steel.

Acknowledgments

The authors would like to thank EPSRC and Tata Steel UK for funding this work.

ORCID

N. Wint https://orcid.org/0000-0002-9229-5728

References

1. N. Mora, E. Cano, J. M. Bastidas, E. Almeida, and J. M. Puente, *J. Coat. Technol.*, **74**, 53 (2002).
2. I. S. Rees, *EUR 17860 Properties and in Service Performance, Development of Chromium Free Passivation Films for Tin Plate* (Office for Official Publications of European Communities, Luxembourg) (1998).
3. S. A. Katz and H. Salem, *J. Appl. Toxicol.*, **13**, 217 (1993).
4. T. Langård, *Norseth. British Journal of Industrial Medicine.*, **32**, 62 (1975).
5. J. H. O. J. Wijenberg, M. Steegh, M. P. Aarnts, and K. R. Lammers, *J.M.C. Mol. Electrochimica Acta.*, **173**, 819 (2015).
6. 7. J. H. O. J. Wijenberg, *Tata Steel, Method for Manufacturing Chromium-Chromium Oxide Coated Substrates*, Pat. WO 2014/202316, 24 December (2014).
7. D. Del Pianta, J. Frayret, C. Gleyzes, C. Cugnet, J. C. Dupin, and I. Le Hecho, *Electrochim. Acta*, **284**, 234 (2018).
8. M. Leimbach, C. Tschaar, U. Schmidt, and A. Bund, *Electrochim. Acta*, **270**, 104 (2018).
9. V. Protsenko and F. Danilov, *Electrochim. Acta*, **54**, 5666 (2009).
10. K. Cho, V. Shankar Rao, and H. Kwon, *Electrochimca Acta.*, **52**, 4449 (2007).
11. J. T. Qi, T. Hashimoto, J. R. Walton, X. Zhou, P. Skeldon, and G. E. Thompson, *Surf. Coat. Technol.*, **280**, 317 (2015).
12. L. Li, A. L. Desouza, and G. M. Swain, *J. Electrochem. Soc.*, **161**, 246 (2014).
13. F. Pearlstein and V. S. Agarwala, *Plat. Surf. Finish.*, **81**, 50 (1994).
14. B. W. Whitman, L. Li, and G. M. Swain, *J. Electrochem. Soc.*, **164**, 135 (2017).
15. L. Li and G. M. Swain, *Corrosion*, **69**, 1205 (2013).
16. C. A. Matzdorf, W. C. Nickerson Jr, E. N. Beck, A. S. Schwartz, and J. L. Green, *U. S. Patent Application Publication, Non-Chromium Coatings for Aluminum*, US2007/0095436 A1, May 3 (2007).
17. Henkel, "Safety data sheet alodine T 5900 RTU." (2008), http://na.henkel-adhesives.com/product-search-1554.htm?nodeid=8797998448641.
18. Socomore, *Technical Data Sheet Annex Application of SOCOSURF TCS/.*, **1**, 1, http://socomore.com/socosurf-tcs-socosurf-pacs/pr387.html.
19. B. Boelen, H. den Hartog, and H. van der Weijde, *Prog. Org. Coat.*, **50**, 40 (2004).
20. H. N. McMurray and G. Williams, "2.14 underfilm/coating corrosion." *Corrosion in Liquids, Types of Corrosion in Liquids, Shreir's Corrosion, 2009*, ed. T. A. J. Richardson (Elsevier, United Kingdom) 4th ed., 2, p. 988 (2016).
21. C. Melvin, E. Jewell, A. C. A. deVooys, K. Lammers, and H. N. McMurray, *Journal of Packaging Technology and Research.*, **2**, 93 (2018).
22. C.-E. Lu, N.-W. Pu, K.-H. Hou, C.-C. Tseng, and M.-D. Ger, *Appl. Surf. Sci.*, **282**, 544 (2013).
23. B. W. Whitman, L. Li, and G. M. Swain, *Appl. Surf. Sci.*, **282**, 544 (2013).
24. F. M. Queiroz, C. R. Tomachuk, E. Zumelzu, H. G. de Melo, and I. Costa, *ECS Trans.*, **43** (2012).
25. G. O. Ilevbare and J. R. Scully, *J. Electrochem. Soc.*, **148**, B196 (2001).
26. T. P. Moffat, H. Yang, F. F. Fan, and A. J. Bard, *J. Electrochem. Soc.*, **139**, 3158 (1992).
27. J. E. Edy, H. N. McMurray, K. R. Lammers, and A. C. A. deVooys, *Corros. Sci.*, **157**, 51 (2019).
28. B. Navinsek, P. Panjan, and I. Milosev, *Surf. Coat. Technol.*, **116–119**, 476 (1999).
29. B. Schuhmacher, W. Muschenborn, M. Stratmann, B. Schultrich, C.-P. Klages, M. Kretschmer, U. Seyfert, F. Forster, and H.-J. Tiller, *Adv. Eng. Mater.*, **3**, 681 (2001).
30. B. Schuhmacher, C. Schwerdt, U. Seyfert, and O. Zimmer, *Surf. Coat. Technol.*, **163–164**, 703 (2003).
31. J. L. Daure, M. J. Carrington, P. H. Shipway, D. G. McCartney, and D. A. Stewart, *Surf. Coat. Technol.*, **350**, 40 (2018).
32. H. B. Liu, J. Tao, J. Xu, Z. F. Chen, and Q. Gao, *Surf. Coat. Technol.*, **204**, 28 (2009).
33. X. L. Pang, K. W. Gao, F. Luo, Y. Emirov, A. A. Levin, and A. A. Volinsky, *Thin Solid Films*, **517**, 1922 (2009).
34. G. J. Reynolds, Z. S. Barrett, H. N. McMurray, and G. Williams, *Corros. Sci.*, **70**, 82 (2016).
35. N. Wint, Z. Barrett, H. N. McMurray, and G. Williams, *J. Electrochem. Soc.*, **167**, 021502 (2020).
36. M. Stratmann, R. Feser, and A. Leng, *Electrochim. Acta*, **39**, 1207 (1994).
37. A. Leng, H. Streckel, and M. Stratmann, *Corros. Sci.*, **41**, 547 (1999).
38. A. Leng, H. Streckel, and M. Stratmann, *Corros. Sci.*, **41**, 579 (1999).
39. A. Leng, A.,. H. Streckel, K. Hoffman, and M. Stratmann, *Corros. Sci.*, **41**, 599 (1999).
40. G. Williams and G.,. H. N. McMurray, *J. Electrochem. Soc.*, **148**, B377 (2001).
41. X. L. Pang, K. W. Gao, F. Luo, Y. Emirov, A. A. Levin, and A. A. Volinsky, *Thin Solid Films*, **517**, 1922 (2009).
42. H. B. Liu, J. Tao, J. Xu, Z. F. Chen, and Q. Gao, *Surf. Coat. Technol.*, **204**, 28 (2009).
43. H. N. McMurray and G. Williams, *J. Appl. Phys.*, **91**, 1673 (2002).
44. G. Williams, C. Kousis, H. N. McMurray, and P. Keil, *Npj Mater Degrad.*, **3**, 41 (2019).
45. U. R. Evans, *Proceedings of the Royal Society of London. Series A, Containing Papers of a Mathematical and Physical Character.*, **107**, 228 (1925).
46. M. Pourbaix, *Atlas of Electrochemical Equilibria in Aqueous Solutions* (Pergamon, Oxford) (1966).
47. N. Agmon, *Chem. Phys. Lett.*, **319**, 247 (2000).
48. W. Furbeth and M. Stratmann, *Fresenius' Journal of Analytical Chemistry.*, **353**, 337 (1995).
49. W. Furbeth and M. Stratmann, *Corros. Sci.*, **43**, 207 (2001).
50. M. Julkarnain, J. Hossain, K. S. Sharif, and K. A. Khan, *J. Optoelectron. Adv. Mater.*, **13**, 485 (2011).